Journal of Low Temperature Physics, Vol. 136, Nos. 5/6, September 2004 (© 2004)

Carbon Nanotube Radio-Frequency Single-Electron Transistor

Leif Roschier, Mika Sillanpää, Wang Taihong*, Markus Ahlskog†, Sumio Iijima‡, and Pertti Hakonen

Helsinki University of Technology, Low Temperature Laboratory, P.O.BOX 2200, FIN-02015 HUT, Finland
**Institute of Physics, Chinese Academy of Sciences, P.O.BOX 603, Beijing 100080, China*
† New permanent address: University of Jyväskylä, Department of Physics P.O.BOX 35, FIN-40014 YFL, Finland
‡ NEC Corporation, 34 Miyukigaoka, Tsukuba, Ibaraki 305-8501, Japan

We discuss the theory of the radio-frequency single-electron transistor and the measurements that use multiwalled carbon nanotubes as active elements. Our devices made of plasma-enhanced chemical-vapor-deposition nanotubes yield charge sensitivities of 10–20 $\mu e/\sqrt{Hz}$.

PACS numbers: 73.23.Hk, 73.63.Fg, 85.35.Gv, 85.35.Kt.

1. INTRODUCTION

The single-electron transistor (SET) is the most sensitive charge detector known to date.[1] Ordinary metallic SETs can detect a charge variation of $3\times10^{-4}e/\sqrt{\text{Hz}}$ at 10 Hz.[2] At low frequencies the sensitivity is limited by the $1/f$-noise, either by background charge fluctuation[3] or variation in tunneling resistance.[4] It has been demonstrated at low frequencies[5] that carbon nanotube SETs can have a higher charge sensitivity by a factor ten compared with the metallic ones, presumably due to the increased distance of the island from the charge fluctuators residing in the SiO_x substrate.[5]

At low frequencies, there are two prevailing ways to read out a charge signal detected by the SET. One alternative is to voltage bias the SET and to measure the current that depends on the island charge. The other choice is to current bias the SET and to measure the voltage. In both cases, the maximum signal bandwidth is set by the RC time, where R is the SET

0022-2291/04/0900-0465/0

resistance and C is the shunting capacitance of the measurement leads. Using practical values of the shunting capacitance $C \sim 0.1$ nF and a SET resistance of $\sim$ 50–200 kΩ, the bandwidth is at most on the order of 100 kHz. In 1998, it was demonstrated that a SET may be read with an increased bandwidth $\sim$ 100 MHz.[6] Instead of measuring voltage or current, the power dissipation was measured. Also, a better charge sensitivity was proved at high frequencies, where the $1/f$-noise did not set the noise floor as in the case of the direct DC biased schemes.[6,7] The measurement setup was named a radio-frequency single-electron transistor (RF-SET). The major advantages of the RF-SET read-out are the wide bandwidth and the high charge sensitivity. The wide bandwidth means, in practice, that also conductance measurements may be carried out orders of magnitude faster compared with the conventional low-frequency lock-in technique.

Recently it has been demonstrated that a superconducting SET may be read also by measuring its inductance at radio frequencies.[8] This low dissipation configuration probably displaces in the future the RF-SET in some applications.

This paper discusses a simple theoretical model for the RF-SET, including the fundamental limits due to Bode–Fano criteria.[9] The estimates for charge sensitivity according to the developed theory agree with the measured charge sensitivity values taken from literature. SETs made of multi-walled carbon nanotubes (MWNT) are discussed, as well as the cryogenic apparatus that was used to measure their electric transport properties. The measured conductance characteristics from reflection measurements are presented. The MWNT RF-SET charge sensitivity measurements are discussed.

2. THEORY

The single-electron transistor (SET) is simply a piece of conductor called "island" that is coupled capacitively to a gate electrode and to the drain and source electrodes via tunnel junctions having tunnel resistance higher than $h/4e^2 \approx 6.5$ kΩ.[1] In this configuration, the total island charge may change only by tunnelling of single electrons with charge e.[1] The SET operation as a transistor is due to the varying gate charge that controls the device conductance. In simple linear approximation, a SET may be considered as a charge controlled resistance.

The basic principle of the RF-SET is illustrated in Fig. 1. A carrier wave is reflected from the impedance transformer circuit and the SET. The variation of the island charge changes the impedance of the SET and the amplitude of the reflected wave is modulated according to these changes. The

optimal charge sensitivity is achieved when there is a perfect power match between the SET and the characteristic impedance of the transmission line. The RF-SET bandwidth is limited by the loaded Q-factor of the impedance transformer.

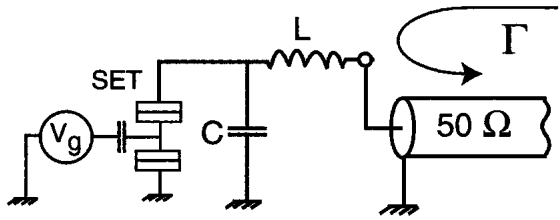

Fig. 1. RF-SET setup. An electromagnetic wave from a transmission line is reflected from the combination of an LC-circuit and the SET. Tuning of the gate voltage changes the resistance of the SET, which modulates the amplitude of the reflection coeffient Γ of the reflected wave.

2.1. Bode–Fano Criteria

The theoretical maximum bandwidth for the case of good power matching may be studied with the help of the Bode–Fano criterion.[9] It states that a resistor R shunted by a capacitance C may be matched to an arbitrary impedance by a lossless matching network with the following constraint[9]

$$\int_0^\infty \ln \frac{1}{|\Gamma(\omega)|} d\omega \leq \frac{\pi}{RC}, \tag{1}$$

where $\Gamma(\omega)$ is the reflection coefficient looking into the matching network as specified in Fig. 2. The definition for the reflection coefficient Γ is

$$\Gamma = \frac{Z_L - Z_T}{Z_L + Z_T}. \tag{2}$$

As a simple example closely related to the RF-SET: a matching network with $\Gamma(\omega) = 0.1$ inside a limited band $\Delta\omega$, and $\Gamma(\omega) = 1$ elsewhere, would have $\Delta\omega \leq \pi/(2.3RC)$. In other words, at most inside the frequency band $\Delta\omega \lesssim 1.36/RC$ power may be exchanged between the RC circuit and the external impedance. Because the best charge sensitivity is attained when Γ

is zero, the shunting capacitance C should be as small as possible in order to maximize $\Delta\omega$. In practice, the capacitance value is set by the bonding pad size of the SET chip and it is on the order of $\gtrsim 0.2$ pF. Consequently, the theoretical maximum bandwidth is $\sim$ 140 MHz with a good match ($\Gamma = 0.1$), $C = 0.2$ pF and $R = 50$ kΩ. In order to increase the bandwidth further, the effect of the bonding pad capacitance can be minimized by using on-chip inductors.

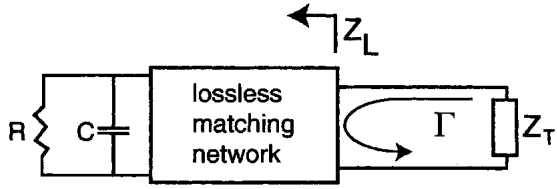

Fig. 2. Circuit to specify the Bode–Fano criteria. Impedance Z may be matched to the resistance R, shunted by the capacitance C, only in a limited band given by Eq. (1). The quality of matching is characterized by the reflection coefficient Γ, defined in Eq. (2).

2.2. Reflection Measurement

The quality of the SET electrometer is judged by its charge sensitivity. In order to estimate it, we need to find the equations of motion to describe the dynamics of the circuit. The classical equations of motion for the circuit depicted in Fig. 3, including the transmission line, are found by using an analysis similar to the one in Ref. 10. In our analysis, both the matching circuit and the SET are treated as lumped elements. The Lagrangian for the circuit is obtained in the following way. For a transmission line with distributed capacitance C_T and inductance L_T the Lagrangian density is written in terms of the phase $\phi_t(x,t) \equiv \int_0^t V(x,t)dt$:

$$\mathcal{L} = \frac{1}{2}\left(C_T\dot{\phi_t}^2 - \frac{1}{L_T}(\frac{\partial\phi_t}{\partial x})^2\right). \tag{3}$$

The use of the Euler–Lagrange equation

$$\frac{d}{dt}\left(\frac{\partial\mathcal{L}}{\partial\dot{\theta}}\right) + \frac{d}{dx}\left(\frac{\partial\mathcal{L}}{\partial(\partial\theta/\partial x)}\right) - \frac{\partial\mathcal{L}}{\partial\theta} = -\frac{\partial D}{\partial\dot{\theta}} \tag{4}$$

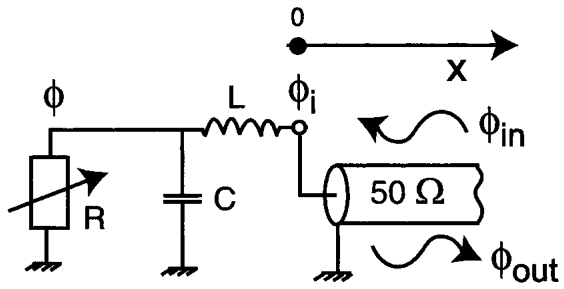

Fig. 3. RF-SET setup for the theoretical analysis. The equations of motion are found for the phases ϕ and ϕ_i which are related to the incoming wave ϕ_{in} and outgoing wave ϕ_{out} according to the analysis in the text. The axis of the x-coordinate of the transmission line is depicted in order to define the point $x = 0$. The SET is approximated as a gate charge controlled resistor.

with $\mathcal{L}$ of Eq. (3) and by using the substitution $\theta \to \phi_t$, gives the wave equation:

$$C_T\ddot{\phi}_t - \frac{1}{L_T}\frac{\partial^2\phi_t}{\partial x^2} = 0, \tag{5}$$

that has a general solution

$$\phi_t(x,t) = \phi_{in}(x/v + t) + \phi_{out}(-x/v + t), \tag{6}$$

where the wave velocity $v^{-1} \equiv \sqrt{L_T C_T}$. In the case above we took $R \to \infty$ in the dissipation function $D \equiv \dot{\theta}^2/2R$.

The point, where the coaxial cable connects to the inductor L is taken as $x = 0$ for the coordinate axis. We define $\phi_i \equiv \phi_t(0,t) = \phi_{in}(t) + \phi_{out}(t)$. The circuit in Fig. 3 has in general two fluxes $\phi(t)$ and $\phi_t(x,t)$. The goal is to find the equations of the motions for the fluxes ϕ, ϕ_i and ϕ_{in} in order to be able to calculate how the reflected wave is related to the incoming wave: $\dot{\phi}_{out}/\dot{\phi}_{in} = (\dot{\phi}_i - \dot{\phi}_{in})/\dot{\phi}_{in}$. ϕ_{in} acts as the driving force in the measurement. In our analysis we calculate its value by fixing the amplitude ϕ over the resistance R (SET), that is linearly related to the charging energy of the SET and sets the scale of all the fluxes.

The total Lagrangian density of the circuit of Fig. 3 is

$$\mathcal{L} = \delta(x)\Big(\frac{1}{2}C\dot{\phi}^2 - \frac{1}{2L}(\phi_i - \phi)^2\Big) + H(x)\Big(\frac{C_T}{2}\dot{\phi}_t^2 - \frac{1}{2L_T}\Big(\frac{\partial\phi_t}{\partial x}\Big)^2\Big), \tag{7}$$

where $\delta(x)$ is the Dirac delta function and $H(x)$ the Heaviside function. By inserting Eq. (7) into Eq. (4) and using the Euler–Lagrange equations with

respect to both ϕ and ϕ_t, we find pair of equations involving ϕ and ϕ_t. The equations are

$$\delta(x)\Big(C\ddot{\phi} + \frac{\dot{\phi}}{R} + \frac{1}{L}(\phi - \phi_i)\Big) = 0. \tag{8}$$

and

$$\delta(x)\frac{1}{L}(\phi_i - \phi) + H(x)C_T\ddot{\phi}_t(x,t) - \frac{1}{L_T}\frac{d}{dx}\Big(H(x)\frac{\partial\phi_t}{\partial x}\Big) = 0. \tag{9}$$

In order to obtain the coupled dynamics of ϕ and ϕ_i we integrate the Eqs. (8) and (9) from $-\epsilon$ to ϵ and take the limit $\epsilon \to 0$ which yields the result for the latter equation:

$$\frac{1}{L}(\phi_i - \phi) - \frac{1}{L_T}\frac{\partial\phi_t}{\partial x}\Big|_{x=0^+} = 0. \tag{10}$$

With the help of the general solution of the wave equation, Eq. (6), we obtain

$$-\frac{1}{L_T}\frac{\partial\phi_t}{\partial x}\Big|_{x=0^+} = \frac{1}{Z_T}\Big(\frac{\partial\phi_i}{\partial t} - 2\frac{\partial\phi_{in}}{\partial t}\Big), \tag{11}$$

where $Z_T = \sqrt{L_T/C_T}$ is the characteristic impedance of the transmission line. Thus, equations of motion for ϕ and ϕ_i become

$$\frac{1}{L}(\phi_i - \phi) + \frac{\dot{\phi}_i}{Z_T} = \frac{2\dot{\phi}_{in}}{Z_T} \tag{12}$$

$$C\ddot{\phi} + \frac{\dot{\phi}}{R} + \frac{1}{L}(\phi - \phi_i) = 0. \tag{13}$$

These equations, independent of the x, are easy to solve and the results can be directly related to reflection measurements. The measured scattering parameter $S_{11}(\omega)$ is the complex Fourier component of the term $\dot{\phi}_{out} = \dot{\phi}_i - \dot{\phi}_{in}$ at frequency ω divided by the Fourier component of the sinusoidal excitation $\dot{\phi}_{in}$ at the same frequency.

2.3. Single Tone Excitation

The basic principle of the RF-SET electrometer is that a variation of the gate charge changes the total impedance of the SET. In order to understand the RF-SET amplitude modulation scheme, we take a simplified model by assuming the SET to be a gate-charge-controlled resistor. We neglect the nonlinearities of the circuit in order to get a simple estimation for the charge sensitivity. An analysis involving nonlinearities is found in Ref. 11, which uses the method of harmonic balance.

The gate charge is modulated sinusoidally with frequency ω_m and the SET resistance R is taken to be of the form

$$\frac{1}{R(t)} = \frac{1}{R_0}\Big(1 + m\cos(\omega_m t)\Big), \tag{14}$$

where m is the modulation depth that is linearly related to the amplitude of the gate charge. By assuming the solution of the Eqs. (12) and (13) to be of the form,

$$\phi = \alpha_c \exp(i\omega_0 t) + \alpha_{us}\exp(i(\omega_0+\omega_m)t) + \alpha_{ls}\exp(i(\omega_0-\omega_m)t) \tag{15}$$

$$\phi_i = \alpha_c^i \exp(i\omega_0 t) + \alpha_{us}^i\exp(i(\omega_0+\omega_m)t) + \alpha_{ls}^i\exp(i(\omega_0-\omega_m)t) \tag{16}$$

$$\phi_{in} = \alpha_c^{in}\exp(i\omega_0 t) \tag{17}$$

with complex coefficients and neglecting higher order mixing products, the equations of the motion may be written using Eqs. (12), (13), (15), (16) and (17) as

$$\mathbf{Ma} = \mathbf{c}\alpha_c, \tag{18}$$

where $\mathbf{M}$ is explicitly

$$\begin{pmatrix} 0 & f(\omega_0+\omega_m) & f(\omega_0-\omega_m) & -\frac{1}{L} & 0 & 0 \\ 0 & g(\omega_0+\omega_m) & 0 & 0 & -\frac{1}{L} & 0 \\ 0 & 0 & g(\omega_0-\omega_m) & 0 & 0 & -\frac{1}{L} \\ -\frac{2i\omega_0}{Z_T} & 0 & 0 & h(\omega_0) & 0 & 0 \\ 0 & -\frac{1}{L} & 0 & 0 & h(\omega_0+\omega_m) & 0 \\ 0 & 0 & -\frac{1}{L} & 0 & 0 & h(\omega_0-\omega_m) \end{pmatrix}, \tag{19}$$

with $f(\omega) \equiv im\omega/2R_0$, $g(\omega) \equiv -C\omega^2 + i\omega/R_0 + 1/L$ and $h(\omega) \equiv 1/L + i\omega/Z_T$. The vectors in Eq. (18) are defined as $\mathbf{a} \equiv (\alpha_c^{in}\ \alpha_{us}\ \alpha_{ls}\ \alpha_c^i\ \alpha_{us}^i\ \alpha_{ls}^i)^T$ and $\mathbf{c} \equiv (-g(\omega_0)\ -f(\omega_0)\ -f(\omega_0)\ 1/L\ 0\ 0)^T$. The indices ls, us and c refer to lower sideband, upper sideband and carrier, respectively. In Eq. (18) the term α_c is on the right hand side, because its amplitude governs the sensitivity of the RF-SET, that is set in practice by the charging energy E_C of the SET. This way we can express the sensitivity in terms of the charging energy. ϕ_{in} term is the incoming wave term and the driving force for Eqs. (12) and (13).

From Eqs. (6), (16) and (17) it is easy to see that

$$\phi_{out}(t) = (\alpha_c^i - \alpha_c^{in})\exp(i\omega_0 t) + \alpha_{us}^i\exp(i(\omega_0+\omega_m)t) + \alpha_{ls}^i\exp(i(\omega_0-\omega_m)t). \tag{20}$$

The first term on the r.h.s. is the carrier and the other two are upper and lower sideband signals that are directly proportional to the modulation index m. The signal may be downconverted either by using a diode detection or by

using a mixer that multiplies the signal with $\cos(\omega_0 t+\gamma)$, where γ is a phase shift that may be experimentally varied. Both methods shift or downconvert the information signal around the carrier frequency ω_c down to frequencies around DC.

Often the signal-to-noise ratio is calculated by comparing the side-peak rms amplitude to the noise floor. In order to extract this value we calculated the vector $\mathbf{a}$ using Eq. (18):

$$\mathbf{a} = \mathbf{M}^{-1}\mathbf{c}\alpha_c. \tag{21}$$

We find the amplitudes of the upper and lower sidebands, in the limit $\omega_m \to 0$:

$$\lim_{\omega_m\to 0}\alpha^i_{us} = \lim_{\omega_m\to 0}\alpha^i_{ls} = \frac{im\alpha_c}{2(\frac{R_0}{Z_{tr}}+Q-i)} \approx \frac{im\alpha_c}{2(\frac{R_0}{Z_{tr}}+\frac{Z_{tr}}{Z_T})}, \tag{22}$$

where the system is characterized with a minimal number of parameters by defining $Q \equiv Z_{tr}/Z_T$, $C = 1/(Z_{tr}\omega_0)$, $L = Z_{tr}/\omega_0$, where $Z_{tr} \equiv \sqrt{L/C}$ is the transformer impedance.

As the side-peak amplitudes α^i_{us} and α^i_{ls} are linearly proportional to the amplitude α_c over the SET, it follows that the side-peak voltage amplitudes are linearly related to the voltage amplitude over the SET, V_s. According to the numerical analysis using "Orthodox theory",[12] leading to the results of Ref. 13, the highest charge sensitivity is achieved with $V_s \approx 0.9E_C/e$, when the preamplifier noise is the dominating noise source, as we assume throughout the article. At this operation point, according our numerical analysis, the effective resistance of the SET is $R_0 \approx 3R_\Sigma$, where R_Σ is the total resistance over the SET at large bias. We define the effective resistance as $\sqrt{\langle V^2\rangle/\langle I^2\rangle}$, where the average $\langle\cdots\rangle$ is taken over a complete AC period. Numerical analysis using "Orthodox theory" yields further the estimation for the modulation index

$$m = \frac{\Delta R}{R_0} = \frac{\partial(R/R_0)}{\partial q}\delta q/e \approx 0.41t^{-1.74}\delta q/e, \tag{23}$$

where $t \equiv T/(E_C/k_B)$ and δq is the amplitude of the gate charge. T is the electron temperature of the SET island. The above numerical formulae are valid over typical values $t = 0.1\ldots0.3$. The lower the value t, the less accurate is the estimation Eq. (23). At $t = 0.3$ the accuracy is good, but at $t = 0.1$ it decreases to 40%. The error is due to the fact that a varying transforming impedance Z_{tr} affects the value of the best operation point. The numerical analysis was calculated for the values 0.5, 1, 1.5, 2 and 2.5 kΩ of the parameter Z_{tr}.

	Ref. 13	Ref. 6	Ref. 14
Z_{tr}	758 Ω	283 Ω	1293 Ω
E_C/k_B	1.13 K	2 K	3.5 K
t	0.33	0.20	0.17
R_Σ	46 kΩ	100 kΩ	43 kΩ
T_0	4 K	10 K	6.3 K
$\delta q_{\rm rms}$ measured	38 $\mu e/\sqrt{\rm Hz}$	47 $\mu e/\sqrt{\rm Hz}$	6.4 $\mu e/\sqrt{\rm Hz}$
$\delta q_{\rm rms}$ estimated	42 $\mu e/\sqrt{\rm Hz}$	75 $\mu e/\sqrt{\rm Hz}$	3.4 $\mu e/\sqrt{\rm Hz}$

Table 1. Parameters for a few normal-state Al RF-SETs including measured and estimated charge sensitivies. The result of Ref. 14 is divided by $\sqrt{2}$, due to the fact that a single SNR of a single side-peak is measured, instead of downconverted signal. The estimates are based on Eq. (25) combined with the heating model.

We find the side-peak voltage amplitudes corresponding to the excitation of e at the gate

$$\sim \frac{0.41t^{-1.74}0.9E_C/e}{2(\frac{3R_\Sigma}{Z_{tr}} + \frac{Z_{tr}}{Z_T})}. \tag{24}$$

In reality the device works at excitation levels of only a fraction of e.

The noise voltage spectral density propagating in the transmission line is $k_B T_0 Z_T$, where T_0 is the noise temperature of the amplifier. It follows that, after detection the charge sensitivity is

$$\delta q_{\rm rms} = \frac{2(\frac{3R_\Sigma}{Z_{tr}} + \frac{Z_{tr}}{Z_T})\sqrt{k_B T_0 Z_T}}{2 \times 0.41t^{-1.74}0.9E_C/e^2} \tag{25}$$

in units of $[e/\sqrt{\rm Hz}]$. The factor 2 in the denominator is due to two facts. A factor $\sqrt{2}$ is because the root-mean-square charge $\delta q_{\rm rms}$ is measured instead of amplitude. Another factor $\sqrt{2}$ is because the information power is in two sidepeaks instead of one.

It is to be noted, that our analysis is similar to the one in Ref. 13, but has less fitting parameters. Different behavior with respect to t may be explained by the slightly different parameter ranges and by the different number of fitting parameters. It is obvious from Eq. (25) that the sensitivity depends strongly on the effective temperature t.

The heating effects have to be taken into account in order to find the effective electron temperature T of the SET island. We use the electron–phonon coupling model $T \sim (P/(2\Sigma\Omega))^{1/5}$,[15] where Σ is a constant of order ~ 1 nW/K$^5/\mu$m^3 and Ω is the volume of the SET island. For the dissipated

power we take $P \approx V_s^2/6R_\Sigma$. Some measured charge sensitivities taken from literature are tabulated in Table 1, along with the values calculated using Eq. (25) and the heating model. The measured charge sensitivities agree with the estimation and the agreement is slightly improved compared with the theory of Ref. 13. The estimation is also more compact than the ones discussed in Refs. 16 and 17, which take the shot noise to be the limiting factor for the sensitivity.

3. CARBON NANOTUBE RF-SET

3.1. Carbon Nanotubes

Carbon nanotubes[18] (CNTs) may be considered as graphene sheets wrapped into the form of a cylinder. There are two types of CNTs: Singlewalled CNTs consist of a single cylinder while multiwalled nanotubes (MWNT) are formed of many concentric tubes inside each other.

The first reports on single-electron charging effects in individual singlewalled CNTs[19] and on bundles of singlewalled CNTs[20] were published in 1997. For singlewalled CNTs on silicon-dioxide substrate, the estimate for Coulomb charging energy due to self-capacitance C_0 is $\frac{e^2}{\epsilon_0 \epsilon L} = 5$ meV$/(L$ [μm]) ,[21] where L is the tube length. Singlewalled CNTs have shown charging energies of 30 meV, that is ~ 300 K in temperature.[21] These CNTs with high charging energy are typically high impedance devices $\gtrsim 1$ MΩ. This is mostly due to the fact that an increase of the contact area between the CNT and the metal electrode lowers the resistance but increases the capacitance and thus also reduces the charging energy.[22] The first published results on Coulomb charging effects on multiwalled nanotubes (MWNTs) were reported in 1999.[23]

According to Eq. (25), a high charging energy enhances the RF-SET sensitivity. MWNTs have a volume smaller than metallic SET islands by a factor $\sim$100–1000 and, thus, their electron temperature increases to a higher value at the same dissipated power level, assuming the electron–phonon coupling coefficients are equal. This increase in temperature decreases the MWNT RF-SET sensitivity according to Eq. (25) in comparison with a metallic device with a similar E_C. It is, however, easier to fabricate a SET with $E_C/k_B \geq 10$ K by using a MWNT as an island than making a similar metallic device using standard electron-beam lithography. Only by using a state-of-the-art electron-beam lithography setup it is possible to fabricate SETs having $E_C/k_B > 10$ K with a reasonable yield.

sample	I	II	Ref. 13
electrodes	over CNT	under CNT	under CNT
AFM manipulated	no	yes	yes
diameter	4 nm	12 nm	16 nm
R_Σ	125 kΩ	400 kΩ	150 kΩ
E_C/k_B	20 K	10 K	3.5 K
t	0.12	0.10	0.22
T_0	5 K	10 K	4 K
length	1.4 μm	1.1 μm	0.8 μm
Z_{tr}	812 Ω	637 Ω	900 Ω
$\delta q_{\rm rms}$ measured	16 $\mu e/\sqrt{\rm Hz}$	19 $\mu e/\sqrt{\rm Hz}$	19 $\mu e/\sqrt{\rm Hz}$
$\delta q_{\rm rms}$ estimated	1.2 $\mu e/\sqrt{\rm Hz}$	9 $\mu e/\sqrt{\rm Hz}$	17 $\mu e/\sqrt{\rm Hz}$

Table 2. Properties of the MWNT RF-SET samples I, II and the sample of Ref. 13. Estimations for the charge sensitivity δq are calculated using Eq. (25) and electron–phonon coupling heating model.

3.2. Manufacturing and Cooling

The electrode structures for our MWNT samples were prepared using standard e-beam lithography. Small, 5×10 mm^2 pieces of a (100) oxidized silicon wafer were used as substrates. Sample I was manufactured by depositing the gold electrodes over the nanotube. Sample II was fabricated by moving a MWNT over prepatterned gold electrodes by using scanning probe manipulation.[24,23] The MWNT material was produced with plasma-enhanced CVD.[25]

The MWNT RF-SET measurements were done with a commercial dilution refrigerator[26] reaching a base temperature of 10 mK. The photograph in Fig. 4 illustrates the parts of the cryostat below 4.2 K and the sample holder for the RF-SET setup. The amplifiers used in the experiments were later replaced by home-made amplifiers[27] that are visible in the picture.

3.3. Experimental Results and Discussion

The high-frequency setup was employed to measure two MWNT samples, denoted by I and II, that showed reasonable Coulomb-charging diamonds. The measurements were done by reflecting a wave from the sample at a low excitation level. The reflected wave amplitude is related to the sample impedance through Eq. (2), where Z_L is the total impedance of the SET and LC-circuit combination and Z_T is the characteristic impedance of

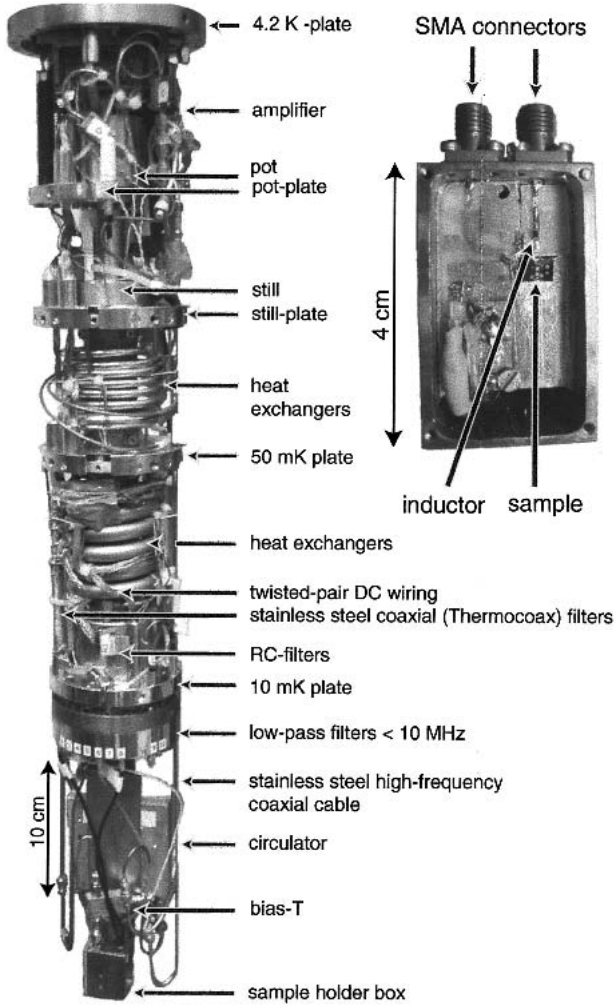

Fig. 4. Left: Photograph of the parts of our high frequency cryostat below 4.2 K. In the measurements, a directional coupler was used instead of the circulator seen in the figure. There is a large space for components to be attached to the 10 mK plate unlike the most cryostats. The cryostat has a "sliding seal" structure, and all the attached components are located inside vacuum. There is a limited space for the components that need to be attached to the 4.2 K plate. In a usual cryostat these components are situated inside the helium bath. Top right: sample holder box (without cover) used for the RF-SET measurements.

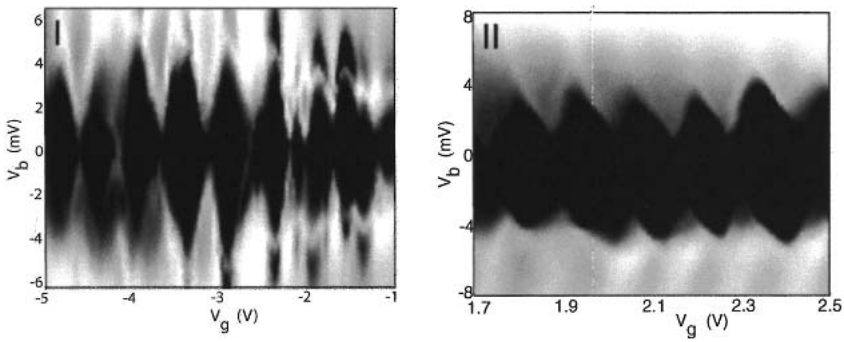

Fig. 5. Reflected wave amplitude on a logarithmic scale, $\log(|\Gamma|)$, as a function of the gate and bias voltages. The lighter the color, the lower the reflection coefficient $|\Gamma|$.

the reflected wave. The sample parameters are listed in Table 2.

Figure 5 depicts two graphs illustrating the reflected wave amplitude as a function of gate and bias voltages. The rhombic patterns are not as symmetric as in the case of metallic SETs, but, nevertheless, the Coulomb-charging diamonds are obvious. In Fig. 5b, the tube features a gap in the conduction around zero bias. In addition we measured nine other MWNTs contacted to the gold electrodes from the same PE-CVD material. None of these samples showed as symmetric diamond patterns as the samples I and II.

In order to test the MWNT RF-SET as an electrometer, we measured the charge sensitivities by injecting a known small AC charge variation in the gate, and optimized the carrier AC amplitude and gate DC bias point to give the highest charge resolution. The values of the measured charge sensitivities are listed in Table 2. The charge sensitivity is calculated from the measured sidepeak signal-to-noise ratio, that is, the side-peak root-mean-square amplitude in comparison with the noise floor SNR set by the preamplifier:

$$\delta q_{\mathrm{rms}} = \frac{\Delta q_{\mathrm{rms}}}{\sqrt{2B}10^{\mathrm{SNR}/20}}. \tag{26}$$

B is the resolution bandwidth of the measurement. The factor $\sqrt{2}$ accounts for the fact that there are two side peaks. Δq_{rms} is the injected charge to the gate that is a fraction of e, typically $e/20$.

The agreement between the estimation of charge sensitivity and the measurements, is not good for samples I and II. Instead, the charge sensitivity of the MWNT sample listed in the Table from Ref. 13, produced with

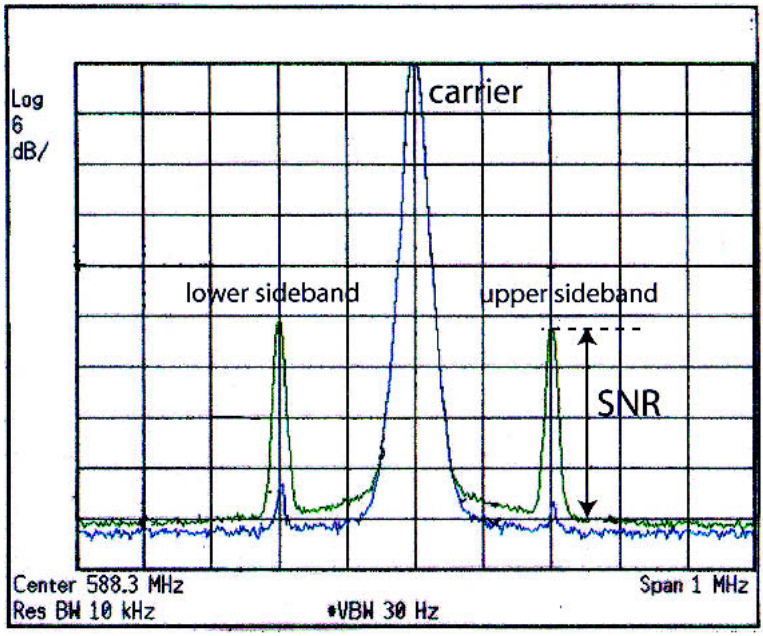

Fig. 6. Typical spectrums of the amplitude modulated signal of sample I. The upper curve corresponds to the optimum charge sensitivity point and the lower curve to a low sensitivity point. It is seen that there is some contribution of the $1/f$-noise, but its effect starts to be dominated by the preamplifier noise at modulation frequencies $\omega_m \geq 100$ kHz. We found the charge noise to follow $1/f$ behavior and a value 400 $\mu e/\sqrt{\text{Hz}}$ at 20 Hz. The frequencies are $\omega_m/2\pi = 200$ kHz and $\omega_0/2\pi = 588.3$ MHz. The biggest peak at the center corresponds to the reflected carrier signal. The sidepeaks corresponds to the gate charge excitation of $1/20e$. The SNR is the ratio between the signal and the noise floor.

the arc-discharge method at the University Montpellier II, fits well to the theory. The discrepancy between the theory and the measurements, with sample I and II, is possibly due to the MWNT current–voltage curves that diverge from the ideal SET curves, that were used in the calculations. It was also found later that the directional coupler was malfunctioning and this may also result for the discrepancy, especially on sample I.

As a conclusion, we have presented a theory to describe the dynamics of the RF-SET. It was used to estimate charge sensitivities that agreed well with the values taken from the literature for Al RF-SET. MWNT RF-SET system was demonstrated and the Coulomb modulation of conductance curves was measured by using the reflection measurement technique. Even though the measurements did not perfectly fit to the theory, nevertheless, they proved that carbon nanotubes may be used to detect charge by using amplitude modulation and that charge sensitivities 10–20 $\mu e/\sqrt{\text{Hz}}$ can be obtained in a straight forward way.

ACKNOWLEDGEMENTS

Financial support by Academy of Finland, by Helsinki University of Technology, by TEKES, and by the Large Scale Installation Program ULTI-III of the European Union (HPRI-1999-CT-00050) is gratefully acknowledged.

REFERENCES

1. K.K. Likharev, *P. IEEE* **87**, 606 (1999).
2. V. Bouchiat, *Quantum fluctuations of the charge in single electron and single Cooper pair devices*, PhD thesis, CEA-Saclay (1997).
3. B. Starmark, T. Henning, T. Claeson, P. Delsing, and A.N. Korotkov, *J. Appl. Phys.* **86**, 2132 (1999).
4. V. Krupenin, D. Presnov, M. Savvateev, H. Scherer, A. Zorin, and J. Niemeyer, *J. Appl. Phys.* **84**, 3212 (1998).
5. L. Roschier, R. Tarkiainen, M. Ahlskog, M. Paalanen, and P. Hakonen, *Appl. Phys. Lett.* **78**, 3295 (2001).
6. R.J. Schoelkopf, P. Wahlgren, A.A. Kozhevnikov, P. Delsing, and D.E. Prober, *Science* **280**, 1238 (1998).
7. P. Wahlgren, *The Radio Frequency Single-Electron Transistor and the Horizon Picture for Tunneling*, PhD thesis, Chalmers University of Technology (1998).
8. M. Sillanpää, L. Roschier, and P. Hakonen, to be published in *Phys. Rev. Lett.*
9. D.M. Pozar, *Microwave engineering*, Addison-Wesley, New York, 1st edition (1990).
10. B. Yurke and J.S. Denker, *Phys. Rev. A* **29**, 1419 (1984).

11. A.N. Korotkov and M.A. Paalanen, *Appl. Phys. Lett.* **74**, 4052 (1999).
12. D.V. Averin and K.K. Likharev, in B.L. Altshuler, P.A. Lee, and R.A. Webb, editors, *Mesoscopic Phenomena in Solids*, page 173, Elsevier (1991).
13. L. Roschier, P. Hakonen, K. Bladh, P. Delsing, K.W. Lehnert, L. Spietz, and R. Schoelkopf, *J. Appl. Phys.* **95**, 1274 (2004).
14. A. Aassime, D. Gunnarsson, K. Bladh, P. Delsing, R. Schoelkopf, *Appl. Phys. Lett.* **79**, 4031 (2001).
15. R.L. Kautz, G. Zimmerli, and J.M. Martinis, *J. Appl. Phys.* **73**, 2386 (1993).
16. V.O. Turin and A.N. Korotkov, *Appl. Phys. Lett.* **83**, 2898 (2003).
17. V.O. Turin and A.N. Korotkov, cond-mat/0308218.
18. S. Ijima, *Nature (London)* **354**, 56 (1991).
19. S.J. Tans, M.H. Devoret, H. Dai, A. Thess, R.S. Smalley, L.J. Geerlings, and C. Dekker, *Nature (London)* **386**, 474 (1997).
20. M. Bockrath, D.H. Cobden, P.L. McEuen, N.G. Chopra, A. Zettl, A. Thess, and R.E. Smalley, *Science* **275**, 1922 (1997).
21. J. Nygård, D.H. Cobden, M. Bockrath, P.L. McEuen, and P.E. Lindelöf, *Appl. Phys. A* **69**, 297 (1999).
22. K. Tsukagoshi, N. Yoneya, S. Uryu, Y. Aoyagi, A. Kanda, Y. Ootuka, and B.W. Alphenaar, *Physica B* **323**, 107 (2002).
23. L. Roschier, J. Penttilä, M. Martin, P. Hakonen, M. Paalanen, U. Tapper, E.I. Kauppinen, C. Journet, and P. Bernier, *Appl. Phys. Lett.* **75**, 728 (1999).
24. M. Martin, L. Roschier, P. Hakonen, Ü. Parts, M. Paalanen, B. Schleicher, and E.I. Kauppinen, *Appl. Phys. Lett.* **73**, 1505 (1998).
25. A. Koshio, M. Yudasaka, and S. Iijima, *Chem. Phys. Lett.* **356**, 595 (2002).
26. LEIDEN CRYOGENICS MNK126-500, LEIDEN CRYOGENICS BV0, 2311 Leiden, The Netherlands, www.leidencryogenics.com.
27. L. Roschier and P. Hakonen, to be published in *Cryogenics*.